Revision

27th November 2015

Generator-Collector Voltammetry at Dual-Plate Gold-Gold Microtrench Electrodes as Diagnostic Tool in Ionic Liquids

Miguel Angel Montiel [1], Jesus Iniesta [1*], Andrew J. Gross [2],
Thies Thiemann [3], and Frank Marken [2*]

[1] University of Alicante, Department of Physical Chemistry and Institute of Electrochemistry, 03080 Alicante, Spain
[2] Department of Chemistry, University of Bath, Claverton Down, Bath, BA2 7AY, UK
[3] United Arab Emirates University, Faculty of Science, Department of Chemistry, Al Ain, United Arab Emirates

To be submitted to Electroanalysis

Proofs to F. Marken

F.Marken@bath.ac.uk

Abstract

Ionic liquids provide high viscosity solvent environments with interesting voltammetric characteristics and new electrochemical mechanisms. Here, a gold-gold dual-plate microtrench electrode is employed in generator-collector mode to enhance viscosity-limited currents in ionic liquids due to fast feedback within small inter-electrode gaps (5 μm inter-electrode gap, 27 μm microtrench depth) and to provide a mechanistic diagnosis tool. Three redox systems in the ionic liquid $BMIm^+BF_4^-$ are investigated: (i) ferrocene oxidation, (ii) oxygen reduction, and (iii) 2-phenyl-naphthyl-1,4-dione reduction. Both transient and steady state voltammetric responses are compared. Asymmetric diffusion processes, reaction intermediates, and solubility changes in the ionic liquid are revealed.

Keywords: ionic liquid, diffusion, oxygen, feedback, sensing, voltammetry.

Graphical Abstract

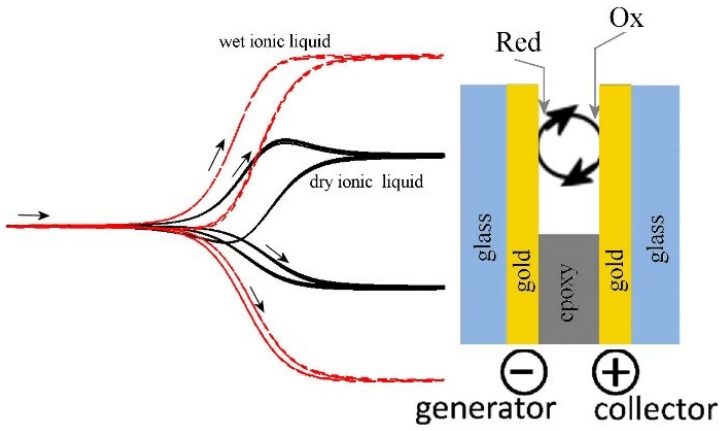

1. Introduction

Ionic liquids have emerged as a family of highly interesting non-volatile solvents [1]. They are now established [2] with many applications in electrochemistry [3,4] and in particular in electroanalysis [5,6]. The benefits of ionic liquids are based on intrinsic ionic conductivity, unusual solubility characteristics, as well as very low volatility [7], which predestine them for applications in gas sensing [8] and in electrochemical metal processing [9]. A wide range of new ionic liquid systems has been developed [10] and some unusual characteristics have emerged such as (i) molecular charge dependent diffusion coefficients with an order of magnitude change observed for example for oxygen and superoxide anions [11], (ii) changes in electron transfer behaviour at the electrode | solution interface when compared to conventional solvent systems [12], and (iii) both agreement [13] and disagreement [14] with Walden's rule when exploring the rate of diffusion as a function of ionic liquid.

In order to work with redox species with a slow rate of diffusion in ionic liquids, it is possible to introduce a second electrode to define a thin diffusion layer region within the inter-electrode gap (see Figure 1). Dual-plate electrode and thin layer devices of this type have been reported previously for applications in electroanalysis usually with micron inter-electrode gap dimension [15,16]. When in generator – collector mode, this type of electrode configuration will result in oxidation and simultaneous reduction at the two opposite plate electrodes to give amplified current signals with steady state (time independent) characteristics. The Nernst layer expression (approximate, based on

the assumption of a large electrode area [17]) for the mass transport controlled limiting current for this kind of dual-plate electrode system can be given (equation 1).

$$I_{\text{lim}} = \frac{DFAc_0}{\delta} \tag{1}$$

In this equation the mass transport limited current I_{lim} is given by D, the diffusion coefficient of the redox active species diffusing towards the electrode, F, the Faraday constant, A, the electrode area, c_0, the sum of the bulk concentrations of oxidised and reduced forms of the redox active species, and δ, the inter-electrode gap. The equation assumes an infinitely extended area and ignores the presence of the "mouth" region, but depending on the depth/aspect ratio of the microtrench electrode the approximation is acceptable. Recent applications of this type of electrode were based on the detection of nitrite and nitrate in serum [18], the suppression of chemically irreversible oxygen or ascorbate interferences [19], the amplified detection of cysteine and cystine [20], chloride determination at a boron-doped diamond dual plate device [15], and the study of several other aqueous redox systems [21] including phosphate transfer at liquid|liquid interfaces [22].

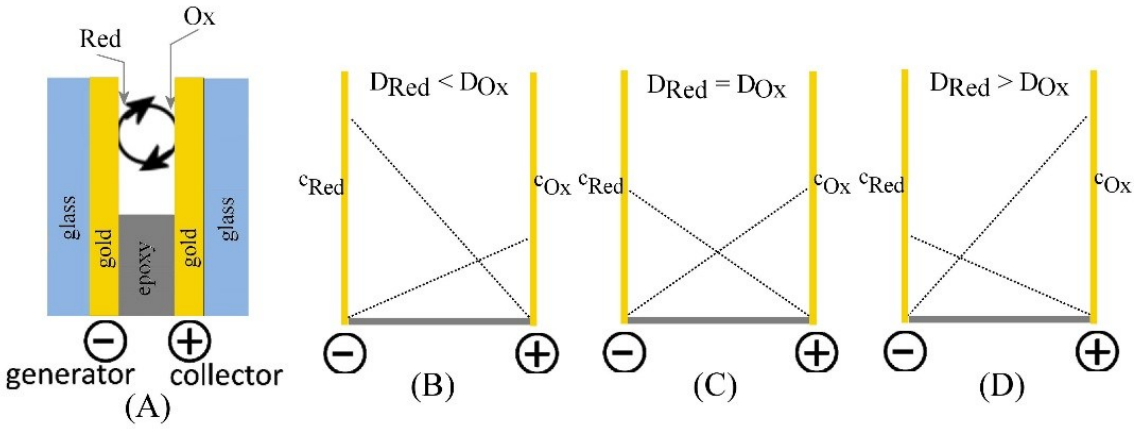

Figure 1. Schematic drawings of the cell and concentration gradients for steady state mass transport limited feedback conditions in generator-collector micro-trench experiments. For unequal diffusion coefficients, the slower diffusion coefficient has a dominant effect on the resulting mass transport controlled limiting current.

In ionic liquids diffusion processes are expected to be considerably slower (compared to those in aqueous media) and additional complexity arises from the fact that in ionic liquids more unequal diffusion coefficients are possible, $D_{\mathrm{Red}} \neq D_{\mathrm{ox}}$. As a result non-symmetric concentration profiles are expected in generator-collector mode under mass transport limited conditions (see Figure 1B-D). Such diffusion effects in ionic liquids have been demonstrated in particular for small molecular redox species including O_2/O_2^- [11], H^+/H_2 [23], and I_2/I_3^- [24]. Due to the slower diffusion coefficient dominating the overall process (and the associated asymmetric concentration distribution between the two electrodes, see Figure 1) interesting new effects are observed and the mass transport limited current expression (equation 2) has to be modified to account for both the slow and the fast diffusion coefficient [25].

$$I_{\mathrm{lim}} = \frac{2FAc_0}{\delta} \frac{D_{red} \times D_{ox}}{D_{red} + D_{ox}} \qquad (2)$$

In this report a gold-gold dual-plate electrode is employed in ionic liquid electrochemistry. Three types of redox probes are studied and compared to demonstrate the underlying complexity in behaviour. The work highlights the limitations of information from voltammetry at a single electrode when compared to information obtained from voltammetry at a dual-plate microtrench electrode. The ferrocene oxidation provides a prototype reaction for the case of a well-defined reversible electron transfer with coupled inter-electrode diffusion. The reduction of oxygen is shown to be more complex with several mechanistic features that lead to less efficient or delayed feedback signals at the collector electrode. Finally, a large organic redox probe molecule, the reduction of 2-phenyl-naphthyl-1,4-dione, is selected as an example of multi-stage electron transfer and additional effects that become apparent only in the micro-trench device. Generator-collector enhanced voltammetric responses are obtained and analysed in terms of reaction diagnostics in all cases.

2. Experimental

2.1. Reagents

1-Butyl-3-methylimidazolium tetrafluoroborate $BMImBF_4$ (>99%) was acquired from Iolitec, Ar and O_2 99,999% from Alphagaz, ferrocene (98%), ferrocenemethanol (98%), Na_2SO_4 99.9% (all from Sigma Aldrich). The compound 2-phenylnaphthalene-1,4-dione was synthetized from phenylnaphthalene-1,4-dione and phenylboronic acid according to the procedure of Y. Fujiwara *et al*. [26]. Aqueous solutions were prepared using ultrapure water (demineralized and filtered water taken from a Millipore water purification system) with 18.2 MΩcm resistivity.

2.2. Instrumentation

Scanning Electron Microscopy (SEM) was performed with a Hitachi S3000N equipment. All electrochemical generation-collection experiments were performed in a four-electrode cell configuration using a Bipotentiostat CH Instruments CHI910B. A dual-plate gold-gold microtrench electrode was used as dual working electrode with a Pt wire as counter electrode. In aqueous experiments, the reference electrode was $Hg/HgSO_4$, while in $BMImBF_4$ experiments both, an Ag/AgCl wire immersed in a saturated KCl in $BMImBF_4$ (home-made) or a Pt wire were used as pseudo-reference electrodes.

$BMImBF_4$ was dried under vacuum at 80 ºC for 24 h before each experiment and an Ar flow was maintained over or through the cell during all the experiments. For the ferrocene experiments in wet $BMImBF_4$, a flow of wet Ar was passed over the cell for 30 minutes to give an amount of water in the ionic liquid equal or higher than 5000 ppm versus 100-150 ppm in dry conditions [27]. Before each oxygen reduction experiment, pure O_2 was bubbled through the cell for 1 h and the flow was kept over the cell during the measurements. To obtain an oxygen-free background, $BMImBF_4$ was dried under vacuum at 80 ºC for 24 h and then dry Ar was bubbled through the liquid for 30 minutes before starting the voltammetric measurements. All measurements were performed at 20 +/- 2 ºC.

2.3. Electrode Fabrication and Calibration

The gold-gold dual-plate microtrench electrode was prepared as detailed in recent work [20]. Briefly, a gold coated glass slide (Sigma-Aldrich) was cut into 10 mm × 25 mm pieces. Only the central 5 mm × 25 mm gold stripe is used (the other gold is etched

away). Epoxy (Gurit SP106) was used to bond two opposing electrodes face-to-face, with the epoxy given 1 hour to pre-cure before application of pressure. The base of the micro-trench was sliced off using a diamond cutter and polished using decreasing grits of SiC abrasive paper (Buehler). Finally, the epoxy was etched out using a shallow piranha bath (5:1 sulphuric acid : hydrogen peroxide; 20 minutes with sonication; *warning: this solution is highly corrosive*) to form the microtrench. Electrodes were investigated by scanning electron microscopy (SEM) to determine the inter-electrode gap. Images in Figure 2A are consistent with an average 5 μm distance between the two gold electrodes, each of which are 5 mm long.

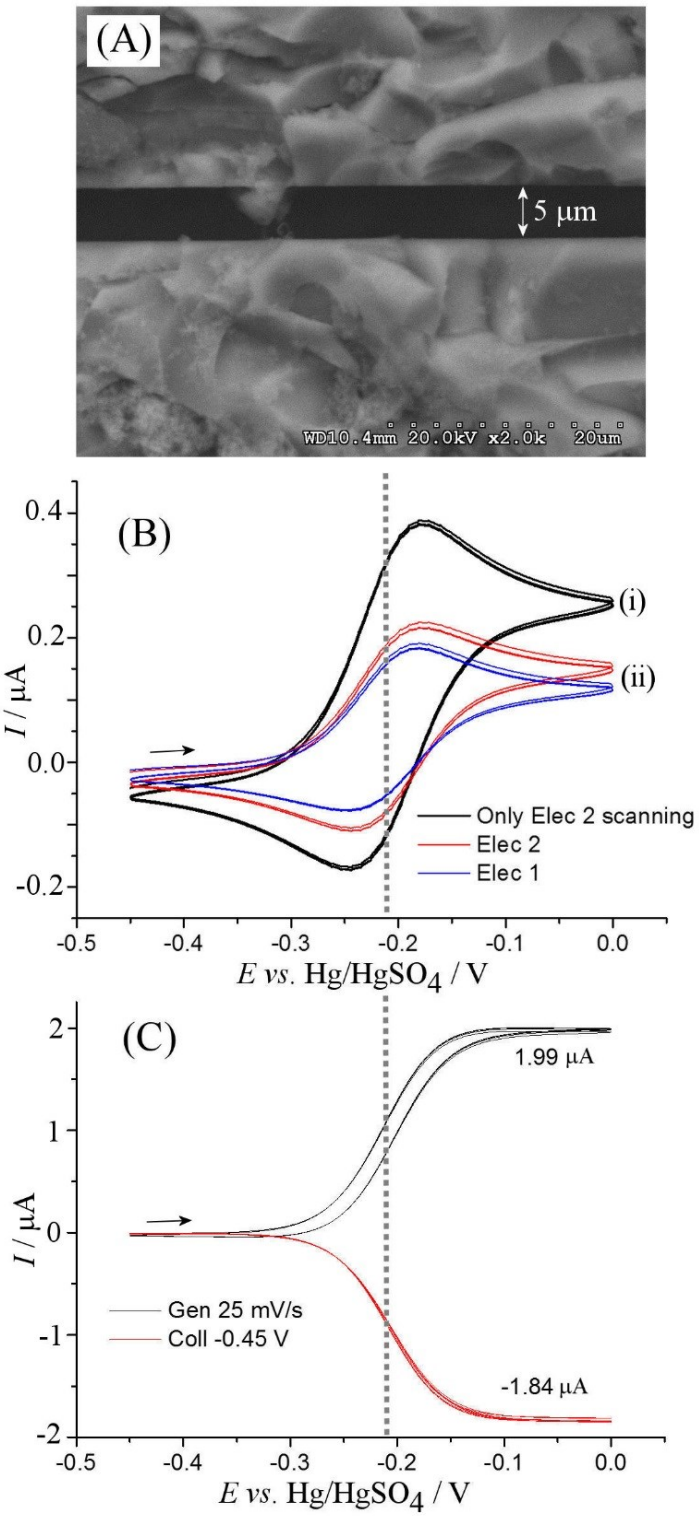

Figure 2. (A) SEM image showing the microtrench with approximately 5 µm inter-electrode gap. (B) Cyclic voltammograms (scan rate 25 mVs^{-1}) obtained for oxidation of 1 mM ferrocenemethanol in 0.1 M Na_2SO_4 for (i) a single electrode connected and (ii) both electrodes independently connected and scanning simultaneously. (C) Cyclic voltammograms (scan rate 25 mVs^{-1}; E_{coll} = -0.45 V vs. $Hg/HgSO_4$) in generator-collector feedback mode.

Before the electrochemical measurements, both gold electrodes were potential cycled between -0.6 and 1.1 V *vs.* $Hg/HgSO_4$ in 0.5 M H_2SO_4 (50 cycles with a scan rate of 100 mVs^{-1}) for the re-conditioning and cleaning of the gold surfaces. The gold-gold dual microtrench electrode and the cell were thoroughly rinsed with pure water and dried under an Ar stream.

In order to calibrate the average depth of the microtrench, the ferrocenemethanol redox probe, 1 mM in aqueous 0.1 M Na_2SO_4, was employed (see Figure 2B). A cyclic voltammogram with only one electrode connected and with a scan rate of 25 mVs^{-1} was recorded showing a typical peak-shaped response (Figure 2B). This result is due to diffusion of redox active species from the solution into the inter-electrode gap (note that the open design of the electrode does not lead to the typical "thin layer" voltammogram [16]). When both electrodes are connected and scanned simultaneously, the individual responses are reduced to about half in magnitude due to competition of the two electrodes. This measurement also shows geometry imperfections with one electrode showing a slightly higher current response (see Figure 2). When scanning one electrode as the generator and fixing the potential of the second electrode at -0.45 V vs. $Hg/HgSO_4$ as the collector, a much enhanced current response is recorded (Figure 2C). The midpoint potentials for both the peak-shaped voltammogram recorded at a single electrode and the sigmoidally-shaped voltammogram recorded under feedback conditions are consistent at -0.21 V vs. $Hg/HgSO_4$ which suggests reversible conditions and mass transport limiting behaviour. With the diffusion coefficient for ferrocenemethanol under these conditions known ($D_{ferrocenemethanol} = 0.6 \times 10^{-9}$ m^2s^{-1} [21]), it is possible to estimate the average microtrench depth as *depth* =

$\frac{I_{lim} \times \delta}{nFD_{ferrocenemethanol} c \times width}$ = 27 μm (based on equation 1). Therefore the aspect ratio of the microtrench is approximately 5.5.

3. Results and Discussion

3.1. Gold-Gold Dual-Plate Microtrench Voltammetry in Ionic Liquid I.: Ferrocene$^{0/+}$

The first ionic liquid redox system under investigation is the oxidation of ferrocene (equation 3). This process has been reported previously [28,29] and is employed here as a highly reversible one-electron redox reaction.

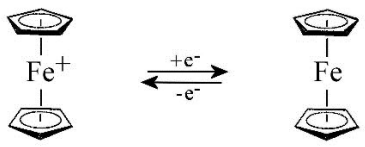

(3)

Figure 3 shows cyclic voltammograms for the oxidation of 5 mM Fc at a gold-gold dual-plate electrode in both dry (vacuum at 80ºC for 24 h, black line) and wet (moisture exposed, red-dashed line) $BMImBF_4$ at a scan rate of 10 mVs^{-1}. Although in dry conditions the generator current response still exhibits peak-shaped features, the collector response is now sigmoidal with a bigger hysteresis loop indicative of a much slower diffusion process [30]. The limiting current for the collector electrode, I_{lim}, can be interpreted in terms of the diffusion coefficients for Fc and Fc^+, with the smaller diffusion coefficient dominating (see equation 2). The viscosity of $BMImBF_4$ is known to decrease dramatically with small amounts of water in the ionic liquid [31] to result in an increased diffusion coefficient for both ferrocene and ferricenium.

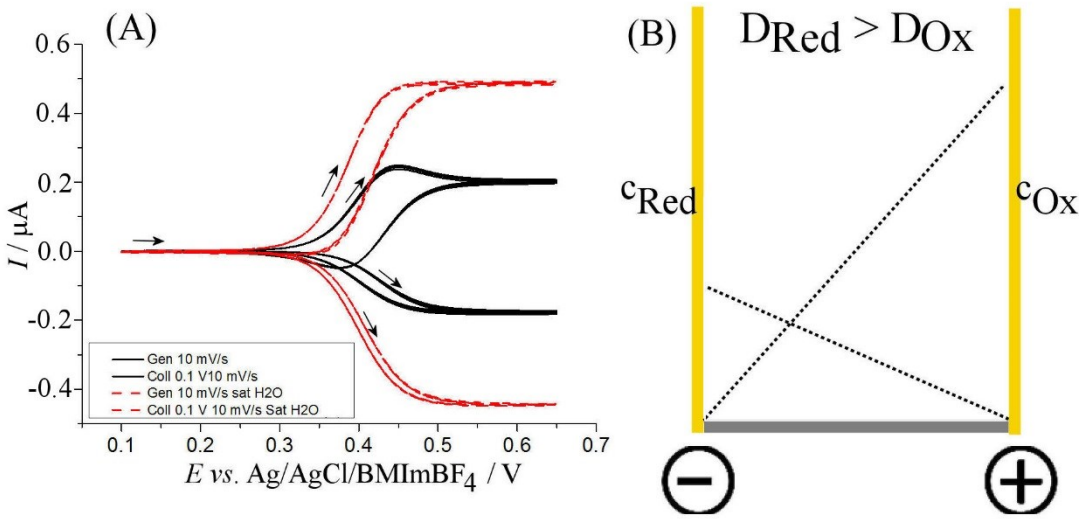

Figure 3. (A) Cyclic voltammograms (Au-Au microtrench, scan rate 10 mVs^{-1}) for 5 mM ferrocene in $BMImBF_4$ vacuum dried (black, approx. 110 ppm water) and exposed to wet Ar (red, over 5000 ppm water [31]). (B) Schematic depiction of the concentration steady state profile for $D_{Red} > D_{Ox}$.

Eisele et al. reported experimental data for D_{Fc} in dry $BMImBF_4$, which were somewhat concentration dependant [32] with D_{Fc} (at 4.3 mM) = 1.3×10^{-11} m^2s^{-1} and D_{Fc} (at 8.6 mM) = 1.8×10^{-11} m^2s^{-1}. Based on equation 1 it is possible to estimate D_{Fc} (at 5 mM) 1.6×10^{-11} m^2s^{-1} in good agreement with the literature report. For the wet $BMImBF_4$ system and employing the same equation, the apparent diffusion coefficient doubles to 3.3×10^{-11} m^2s^{-1}. Both values are likely to be an average with the true diffusion coefficient for ferrocene being higher and the true diffusion coefficient for ferricenium being lower (see equation 2).

The results confirm that dual-plate gold-gold microtrench electrodes provide a good platform for working in viscous ionic liquids and to obtain diffusion coefficient. Next, the collection efficiency and the hysteresis effect (originating from the inter-electrode diffusional time delay) are investigated in more detail. Figure 4 shows cyclic voltammograms obtained with different scan rates for dry and wet $BMImBF_4$. In dry

conditions (Figure 4A), hysteresis effects in the collector response are important both in low and high scan rates. However, the presence of moisture in the ionic liquid, the collector hysteresis effect is considerably decreased (see Figure 4B).

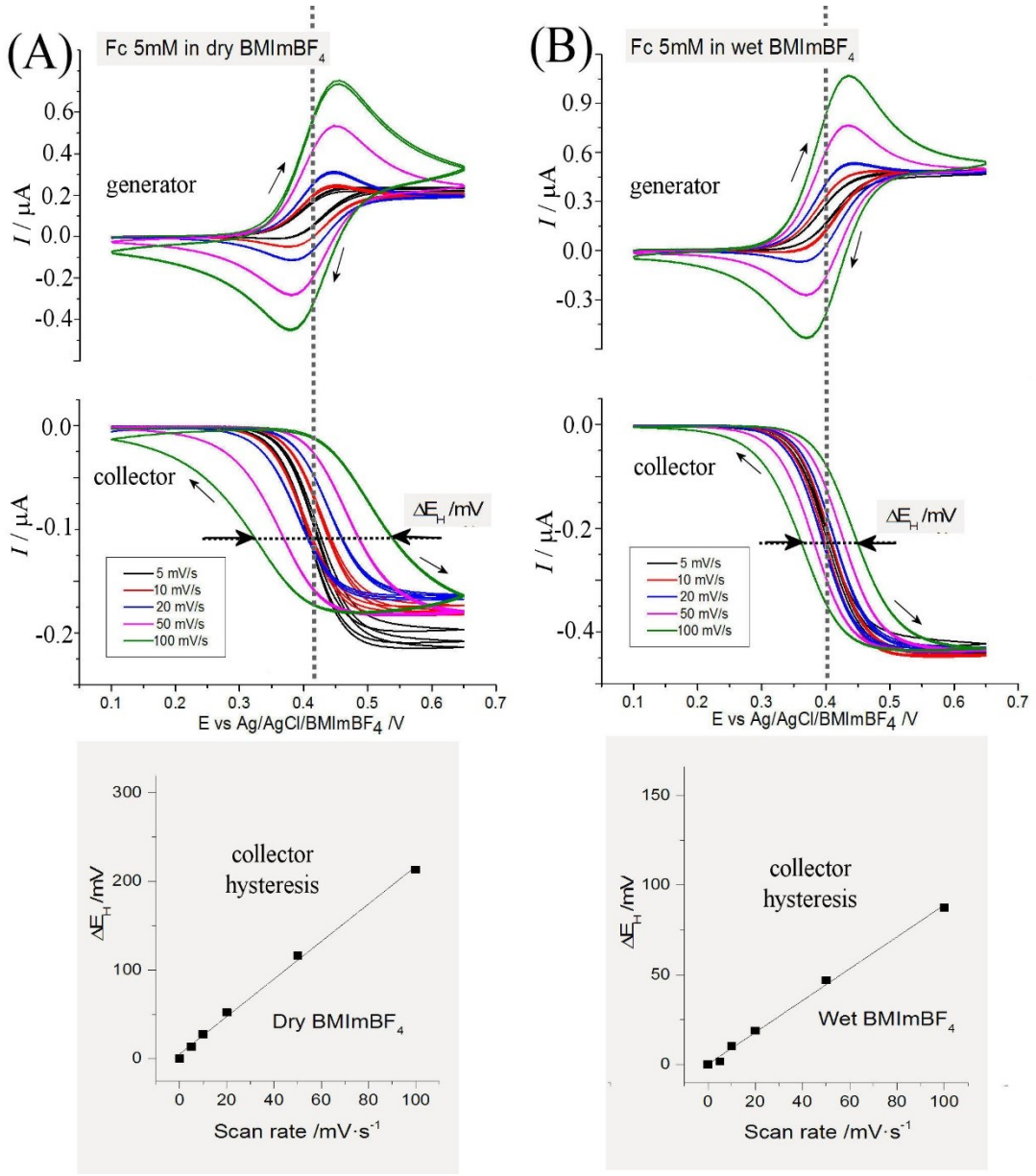

Figure 4. Cyclic voltammograms (Au-Au microtrench, scan rate 5, 10, 20, 50, 100 mVs^{-1}, collector at 0.1 V) for 5 mM ferrocene in $BMImBF_4$ (A) under dry conditions (approx. 110 ppm water) and (B) under wet conditions (approx. 5000 ppm water). Linear plots are shown for the collector response hysteresis effect (mV) versus scan rate (mVs^{-1}).

When comparing the generator and collector data for dry ionic liquid (Figure 4A) and for wet ionic liquid (Figure 4B), it can be seen that the collection efficiency (the ratio of collector limiting current / generator limiting current) in dry conditions is 81% while in wet conditions is 95%. This more subtle difference could be attributed to the aspect ratio of 5.5 (see Experimental) allowing some redox active material to diffuse into the region outside of the inter-electrode gap. The hysteresis effect (see Figure 4) is investigated in both dry and wet $BMImBF_4$ and plotted versus scan rate. Linear trends are observed and the experimental slope can be contrasted with the ideal slope for a one-electron reversible process calculated based on the diffusion coefficient (see equation 4) [25].

$$\frac{\Delta E_{H,experimental}}{\Delta E_{H,ideal}} = \frac{experimental\ hysteresis\ slope}{ideal\ hysteresis\ slope} = \frac{(experimental\ hysteresis\ slope)\ DRT}{0.0071F\delta^2} \qquad (4)$$

In this equation the ideal hysteresis $\Delta E_{H,ideal}$, is expressed in terms of the diffusion coefficient D, the ideal gas constant R, the absolute temperature T, the Faraday constant F and the inter-electrode gap δ. For dry $BMImBF_4$ $\frac{\Delta E_{H,experimental}}{\Delta E_{H,ideal}} = 5$ and in wet $BMImBF_4$ $\frac{\Delta E_{H,experimental}}{\Delta E_{H,ideal}} = 4.2$, which suggests a considerably higher hysteresis effect for both compared to the ideal theoretical value. A higher hysteresis indicates a delay in the development of the diffusion layer concentration profile and this is likely to be linked in this case to $D_{ox} \neq D_{red}$ and the development of a corresponding asymmetric concentration profile (see Figure 3B). This effect appears less strong in the wet ionic liquid.

3.2. Gold-Gold Dual-Plate Microtrench Voltammetry in Ionic Liquid II.: Oxygen Reduction

Oxygen redox chemistry in ionic liquids is of interest fundamentally [33], and in sensor development [34]. The reactivity of oxygen has been studied in different types of ionic liquids and at both platinum and gold electrodes. An ion pairing mechanism due to interaction of superoxide radical anions with imidazolium cations has been observed [35]. Diffusion processes for oxygen in ionic liquids have been carefully assessed [36] and for $BMImBF_4$ at 293 K the diffusion coefficient for oxygen has been determined as 1.26×10^{-10} m^2s^{-1} with a concentration of c_{oxygen} = 4.9 mM (at 293 K). The corresponding diffusion coefficient for the superoxide radical cation is likely to be at least a factor 2 smaller [37].

Data in Figure 5 show generator-collector cyclic voltammograms for de-aerated $BMImBF_4$ (black line) and for O_2 -saturated $BMImBF_4$ (blue line) with a scan rate of 50 mVs^{-1} at a gold-gold dual-plate microtrench electrode. Under these conditions $BMImBF_4$ should have approximately 100-150 ppm of water (dried in vacuum oven for 24 h at 80 ºC), which can still affect the appearance of the cyclic voltammogram. At a negative potential of -1.1 V the O_2 reduction signal appears as a quasi-reversible wave. This reduction process is associated with the formation of the superoxide anion radical (see equation 5) as was previously reported by Compton and coworkers [37]. In the presence of sufficient levels of protons in $BMImBF_4$, superoxide reacts further via dismutation to form oxygen and hydrogen peroxide (see equation 6). The direct reaction of superoxide with the slightly acidic imidazolium cations has also been reported [38]. At more negative applied potentials a further direct reduction of superoxide may also be possible (*vide infra*, equation 7).

$$O_2 + e^- \rightleftharpoons O_2^{\cdot -} \quad (5)$$

$$2\,O_2^{\cdot -} + 2\,H^+ \longrightarrow O_2 + H_2O_2 \quad (6)$$

$$O_2^{\cdot -} + e^- + H^+ \longrightarrow HO_2^- \quad (7)$$

In $BMImBF_4$, the main source of H^+ is the remaining water (and less importantly the slightly acidic proton on the position 2 of the imidazolium ring). The homogenous dismutation reaction can diminish the collection efficiency in generator-collector experiments. Figure 5A shows a collector response associated with the oxygen reduction at -1.1 V, but with a collection efficiency of less than 50%.

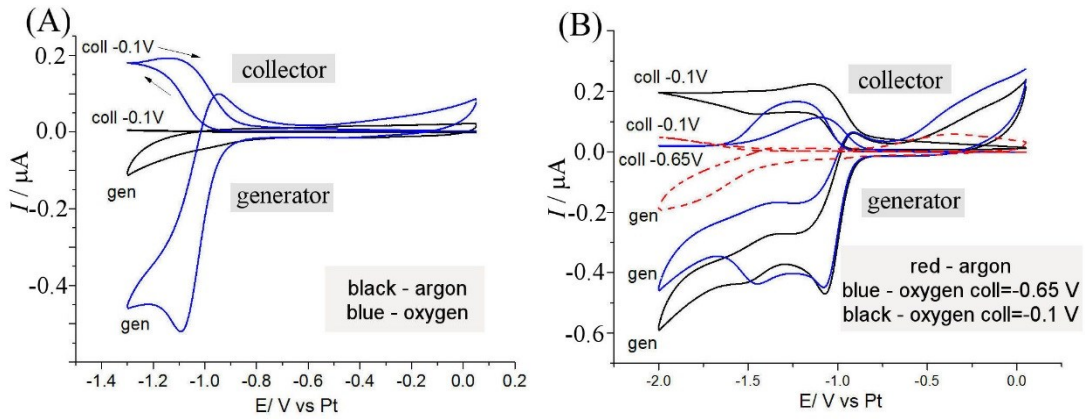

Figure 5. (A) Cyclic voltammograms (scan rate 50 mVs^{-1}, collector potential -0.1 V) in dry $BMImBF_4$ under Ar (black) and after 30 min of O_2 purging (blue). (B) As above, but data recorded over a wider potential window and for collector potentials -0.1 V (black) and -0.65 V (blue) vs. a platinum wire.

Therefore, the O_2 reduction at the generator is successfully collected at the collector at -0.1 V, the collection reaction is assigned to the re-oxidation of the superoxide radical anion to oxygen, but approximately half of the superoxide is reacting further. In order to better explore the effects of generator and collector potentials on the superoxide

reactivity, the potential window is expanded and the generator electrode potential is scanned from 0.0 to -2.0 V (Figure 5B). With the collector potential held at -0.1 V, the collector currents plateaus were fixed at ca. 0.2 μA. However, with the collector potential held at -0.65 V a new process occurs at -1.5 V resulting in loss of the collector response (see equation 7). These results indicate that the superoxide radical anion, once formed at the generator, is collected at both -0.1 V and -0.65 V, but a second species, most likely the peroxide anion HO_2^-, is also collected at -0.1 V but not at -0.65 V. The formation of HO_2^- appears to be possible not only via dismutation but also directly at the gold generator electrode at -1.5 V.

When the collector potential is kept at -0.65 V, only the superoxide radical anion is re-oxidized. To get more quantitative insights into the superoxide generation and collection, experiments are conducted with a restricted potential window from -0.1 V to -1.25 V and from -0.65 V to -1.25 V. Figure 6 shows the oxygen reduction reaction in $BMImBF_4$ at three scan rates, at 20 (blue), 50 (red) and at 100 (green) mVs^{-1} at two different collector potentials, at -0.1V (Figure 6A) and at -0.65 V (Figure 6B).

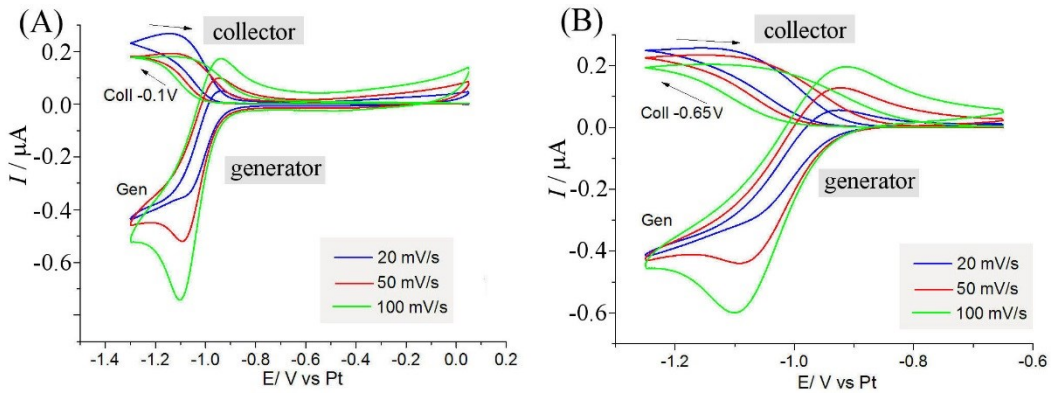

Figure 6. (A) Cyclic voltammograms (scan rate 20, 50, 100 mVs^{-1}, collector potential -0.1 V) for 30 minute O_2 purged $BMImBF_4$. (B) As above but with collector potential at -0.65 V vs. Pt wire.

The mass transport controlled limiting current for oxygen reduction with formation of superoxide and re-oxidation is approximately 0.25 μA (Figure 6B), which compares to the estimated value (based on equation 1 and assuming $D = 1.26 \times 10^{-10}$ m^2s^{-1} and c = 4.9 mM [36]) of 1.6 μA. The loss of superoxide due to dismutation significantly reduces the mass transport controlled limiting current. Also the lower diffusion coefficient for the superoxide radical anion is expected to lower the current (see equation 2). Considerable hysteresis effects are observed with $\frac{\Delta E_{H,experimental}}{\Delta E_{H,ideal}} = 70$ indicative of a complex mechanism with (i) multi-electron character, (ii) a strong imbalance of diffusion coefficients, and/or (iii) additional reactive intermediates.

3.3. Gold-Gold Dual-Plate Microtrench Voltammetry in Ionic Liquid III.: 2-Phenylnaphthyl-1,4-dione Reduction

Benzoquinone reactivity in ionic liquid media has been well-documented [39,40,41,42] and is usually associated with two reduction steps as well as anion-cation association and comproportionation chemistry. Here, the benzoquinone derivative 2-phenylnaphthyl-1,4-dione is investigated as a case of particularly slow diffusion in dry $BMImBF_4$. Initially, the diffusion coefficient D for 2-phenylnaphthyl-1,4-dione is estimated by steady state voltammetry (employing $I_{lim} = 4nFDrc$ [43]) at a 25 μm diameter gold ultramicroelectrode in dry $BMImBF_4$ to give $D = 3.6 \times 10^{-12}$ m^2s^{-1}. This value is a factor 4.4 slower compared to the diffusion coefficient of ferrocene in the same solvent consistent with a considerably larger molecular radius.

Figure 7A shows cyclic voltammetry data for the reduction of 2-phenylnaphthyl-1,4-dione in dry $BMImBF_4$. There are two clear reduction processes denoted P1 and P2, both of which appear to show chemical reversibility consistent with two distinct one-electron reduction steps.

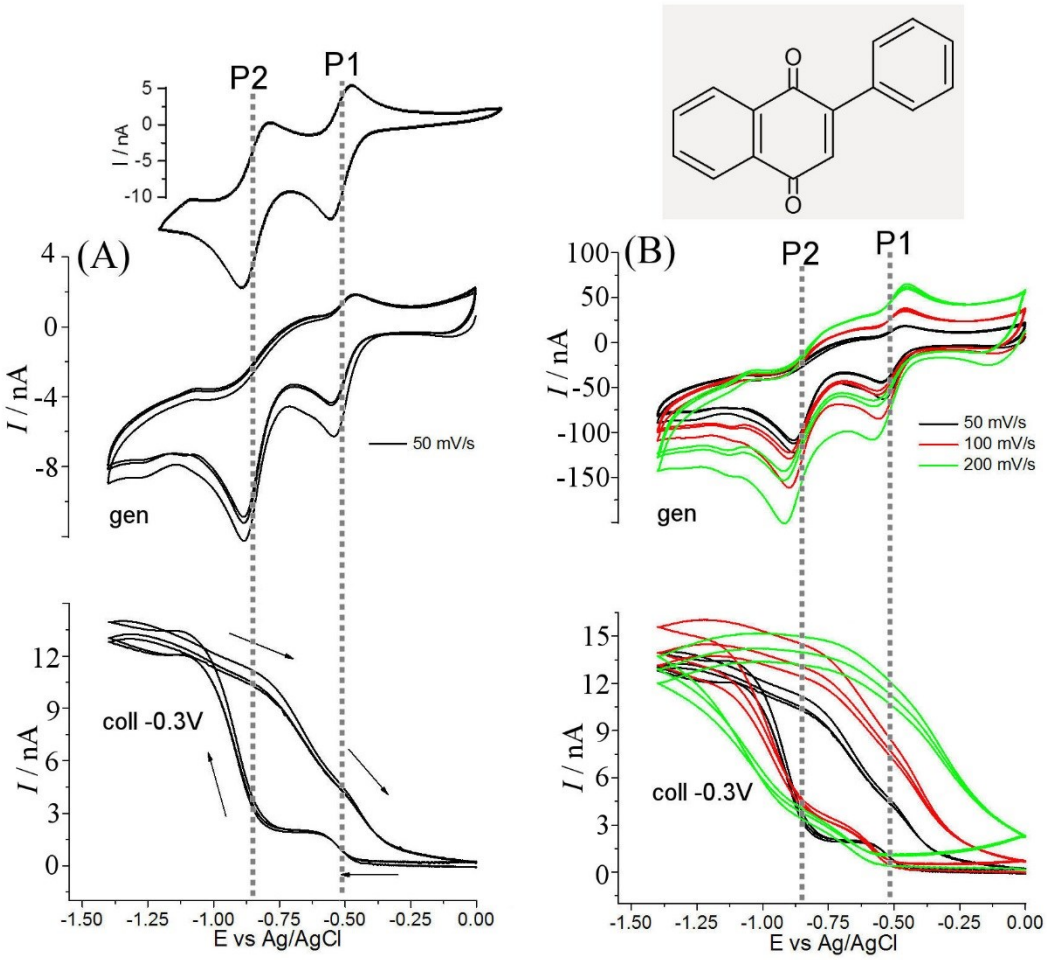

Figure 7. (A) Top: cyclic voltammogram (scan rate 50 mVs^{-1}) for the reduction of 5 mM 2-phenylnaphthyl-1,4-dione in dry $BMImBF_4$ at a 100 μm diameter gold disc electrode. Below: generator-collector gold-gold dual-plate microtrench voltammograms (scan rate 50 mVs^{-1}, three consecutive cycles, collector potential -0.3 V). (B) As above, but for scan rate 50 mVs^{-1} (black), 100 mVs^{-1} (red), and 200 mVs^{-1} (green).

The reduction of 2-phenylnaphthyl-1,4-dione in dry $BMImBF_4$ at a gold-gold dual-plate microtrench electrode (Figure 7A) results in more complex features. At the generator electrode the first and the second reduction steps are clearly detected. Currents at the generator electrode converge towards the mass transport controlled limiting currents estimated based on equation 1: for the first reduction 47 nA and for the second reduction 94 nA. However, when inspecting the collector current responses, it is obvious that much lower limiting currents are associated with the processes P1 and P2. The two main reasons for this non-ideal behaviour could be (i) an insufficiently positive collector potential to drive the oxidation at the mass transport controlled limit or (ii) association processes of the reduced forms of 2-phenylnaphthyl-1,4-dione in dry $BMImBF_4$ causing apparent chemical irreversibility and loss of some fraction of the collector current. Irreversibility is seen also in the generator current where oxidation peaks are lower than expected and therefore loss of redox active material due to aggregation within the microtrench is inferred. From the magnitude of the collector current it can be estimated that approximately 90 % of the reduced 2-phenylnaphthyl-1,4-dione is aggregating. In this case the gold-gold dual-plate microtrench electrode can be employed as diagnosis tool to explore mechanistic features that are not revealed in experiments under the same conditions but with a single electrode.

4. Conclusions

Voltammetric experiments in $BMImBF_4$ have been performed with a gold-gold dual-plate microtrench electrode in generator-collector mode. Although preliminary in nature, data from voltammetry with three redox systems (the oxidation of ferrocene,

reduction of oxygen, and reduction of 2-phenylnaphthyl-1,4-dione) reveal further complexity that is not evident in voltammetry experiments with a single electrode. The generator-collector mode allows fast transport to be imposed (the inter-electrode gap = diffusion layer thickness) and non-ideal behaviour can be assessed by investigating the hysteresis effect and shape of the collector electrode responses under these conditions. This type of dual-plate electrode could also be used to discriminate electrochemically reversible redox processes from irreversible processes [44] in order to selectively sense redox species under fast mass transport conditions and under steady state conditions at the same time.

Acknowledgements

A.J.G and F.M gratefully acknowledge the Engineering and Physical Sciences Research Council (EP/I028706/1) for financial support. M.A.M. and J.I. also thank the financial support from MICINN-FEDER (Spain) through the project CTQ2013-48280-C3-3-R.

References

[1] L.E. Barrosse-Antle, A.M. Bond, R.G. Compton, A.M. O'Mahony, E.I. Rogers, D.S. Silvester, *Chem. Asian J.* **2010**, *5*, 202-230.

[2] D.S. Silvester, E.I. Rogers, L.E. Barrosse-Antle, T.L. Broder, R.G. Compton, *J. Braz. Chem. Soc*. **2008**, *19*, 611-620.

[3] D.S. Silvester, R.G. Compton, *Zeitschrift Physik. Chem. Internat. J. Res. Phys. Chem. Chem. Phys.* **2006**, *220*, 1247-1274.

[4] D.A. Walsh, K.R.J. Lovelock, P. Licence, *Chem. Soc. Rev.* **2010**, *39*, 4185-4194.

[5] D.S. Silvester, *Analyst* **2011**, *136*, 4871-4882.

[6] M.C. Buzzeo, C. Hardacre, R.G. Compton, *Anal. Chem.* **2004**, *76*, 4583-4588.

[7] R. Hagiwara, J.S. Lee, *Electrochem.* **2007**, *75*, 23-34.

[8] L. Xiong, R.G. Compton, *Internat. J. Electrochem. Sci.* **2014**, *9*, 7152-7181.

[9] A.P. Abbott, G. Frisch, J. Hartley, K.S. Ryder, *Green Chem.* **2011**, *13*, 471-481.

[10] H.P. Steinruck, P. Wasserscheid, *Catal. Lett.* **2015**, *145*, 380-397.

[11] P.L. Li, E.O. Barnes, C. Hardacre, R.G. Compton, *J. Phys. Chem. C* **2015**, *119*, 2716-2726.

[12] E.E.L. Tanner, E.O. Barnes, C.B. Tickell, P. Goodrich, C. Hardacre, R.G. Compton, *J. Phys. Chem. C* **2015**, *119*, 7360-7370.

[13] R.G. Evans, O.V. Klymenko, C. Hardacre, K.R. Seddon, R.G. Compton, *J. Electroanal. Chem.* **2003**, *556*, 179-188.

[14] U. Schröder, J.D. Wadhawan, R.G. Compton, F. Marken, P.A.Z. Suarez, C.S. Consorti, R.F. de Souza, J. Dupont, *New J. Chem.* **2000**, *24*, 1009-1015.

[15] A.T. Hubbard, D.G. Peters, *CRC Cr. Rev. Anal. Chem.* **1973**, *3*, 201-211.

[16] T.R.L.C. Paixão, E.M. Richter, J.G.A. Brito-Neto, M. Bertotti, *Electrochem. Commun*. **2006**, *8*, 9–14.

[17] A.J. Gross, F. Marken, *Electrochem. Commun.* **2014**, *46*, 120-123.

[18] A.J. Gross, S. Holmes, S.E.C. Dale, M.J. Smallwood, S.J. Green, C.P. Winlove, N. Benjamin, P.G. Winyard, F. Marken, *Talanta* **2015**, *131*, 228-235.

[19] M.A. Hasnat, A.J. Gross, S.E.C. Dale, E.O. Barnes, R.G. Compton, F. Marken, *Analyst* **2014**, *139*, 569-575.

[20] J.L. Hammond, A.J. Gross, P. Estrela, J. Iniesta, S.J. Green, C.P. Winlove, P.G. Winyard, N. Benjamin, F. Marken, *Anal. Chem*. **2014**, *86*, 6748-6752.

[21] A.J. Gross, F. Marken, *Electroanalysis* **2015**, *27*, 1035-1042.

[22] M. Li, G.E.M. Lewis, T.D. James, Y.T. Long, B. Kasprzyk-Hordern, J.M. Mitchels, F. Marken, ChemElectroChem. 2014, 1, 1640-1646.

[23] Y. Meng, L. Aldous, R.G. Compton, *J. Phys. Chem. C* **2011**, *115*, 14334-14340.

[24] C.L. Bentley, A.M. Bond, A.F. Hollenkamp, P.J. Mahon, J. Zhang, *J. Phys. Chem. C* **2014**, *118*, 22439-22449.

[25] S.E.C. Dale, A. Vuorema, M. Sillanpää, J. Weber, A.J. Wain, E.O. Barnes, R.G. Compton, F. Marken, *Electrochim. Acta* **2014**, *125*, 94-100.

[26] Y. Fujiwara, V. Domingo, I. B. Seiple, R. Gianatassio, M. del Bel, P. S. Baran, *J. Am Chem. Soc.* **2011**, *133*, 3292-3295.

[27] A.M. O'Mahony, D.S. Silvester, L. Aldous, C. Hardacre, R.G. Compton, *J. Chem. Eng. Data* **2008,** *53,* 2884-2891.

[28] C.P. Fu, L. Aldous, E.J.F. Dickinson, N.S.A. Manan, R.G. Compton, *ChemPhysChem* **2011**, *12*, 1708-1713.

[29] L.E. Barrosse-Antle, L. Aldous, C. Hardacre, A.M. Bond, R.G. Compton, *J. Phys. Chem. C* **2009**, *113*, 7750-7754.

[30] A. Vuorema, H. Meadows, N. Bin Ibrahim, J. Del Campo, M. Cortina-Puig, M.Y. Vagin, A.A. Karyakin, M. Sillanpää, F. Marken, *Electroanalysis* **2010**, *22*, 2889-2896.

[31] L.A.S. Ries, F.A. do Amaral, K. Matos, E.M.A. Martini, M.O. de Souza, R.F. de Souza, *Polyhedron* **2008**. *27*, 3287–3293.

[32] S. Eisele, M. Schwartz, B. Speiser, C. Tittle, *Electrochim. Acta* **2006**, *51*, 5304.

[33] E.E.L. Tanner, L. Xiong, E.O. Barnes, R.G. Compton, *J. Electroanal. Chem.* **2014**, *727*, 59–68.

[34] L.H.J. Xiong, E.O. Barnes, R.G. Compton, *Sens. Actuators* **2014**, *200*, 157-166.

[35] E.I. Rogers, X.J. Huang, E.J.F. Dickinson, C. Hardacre, R.G. Compton, *J. Phys. Chem. C* **2009**, *113*, 17811-17823.

[36] X.J. Huang, E.I. Rogers, C. Hardacre, R.G. Compton, *J. Phys. Chem. B* **2009**, *113*, 8953-8959.

[37] M.C. Buzzeo, O.V. Klymenko, J.D. Wadhawan, C. Hardacre, K.R. Seddon, R.G. Compton, *J. Phys. Chem. A* **2003**, *107*, 8872-8878.

[38] M.M. Islam, T. Imase, T. Okajima, M. Takahashi, Y. Niikura, N. Kawashima, Y. Nakamura, T. Ohsaka, *J. Phys. Chem. A* **2009**, *113*, 912-916.

[39] Y.J. Wang, E.I. Rogers, S.R. Belding, R.G. Compton, *J. Electroanal. Chem.* **2010**, *648*, 134-142.

[40] V.A. Nikitina, R.R. Nazmutdinov, G.A. Tsirlina, *J. Phys. Chem. B* **2011**, *115*, 668-677.

[41] S.F. Zhao, J.X. Lu, A.M. Bond, J. Zhang, *Electrochem. Commun.* **2012**, *16*, 14-18.

[42] M.A. Bhat, A. Konar, P.P. Ingole, A.H. Pandith, *J. Phys. Org. Chem.* **2012**, *25*, 1243-1246.

[43] A.J. Bard, L.R. Faulkner, *Electrochemical Methods*, John Wiley, New York, 2001, p. 174.

[44] G.E.M. Lewis, S.E.C. Dale, B. Kasprzyk-Hordern, A.T. Lubben, E.O. Barnes, R.G. Compton, F. Marken, *Phys. Chem. Chem. Phys.* **2014**, *16*, 18966-18973.